

Article

Low-Temperature Migration-Enhanced Epitaxial Growth of High-Quality $(\text{InAs})_4(\text{GaAs})_3/\text{Be}$ -Doped InAlAs Quantum Wells for THz Applications

Linsheng Liu ^{1,†} , Zhen Deng ^{2,†}, Guipeng Liu ³, Chongtao Kong ^{4,5}, Hao Du ¹, Ruolin Chen ¹, Jianfeng Yan ⁶, Le Qin ², Shuxiang Song ¹, Xinhui Zhang ^{4,5,*}  and Wenxin Wang ^{2,*}

- ¹ Guangxi Key Laboratory of Brain-inspired Computing and Intelligent Chips/Key Laboratory of Integrated Circuits and Microsystems (Education Department of Guangxi Zhuang Autonomous Region), School of Electronic and Information Engineering/School of Integrated Circuits, Guangxi Normal University, Guilin 541004, China; linshengliu@mailbox.gxnu.edu.cn (L.L.)
- ² Institute of Physics, Chinese Academy of Sciences, Beijing 100190, China
- ³ School of Physical Science and Technology, Lanzhou University, Lanzhou 730000, China
- ⁴ State Key Laboratory of Superlattices and Microstructures, Institute of Semiconductors, Chinese Academy of Sciences, Beijing 100083, China
- ⁵ Center of Materials Science and Optoelectronics Engineering, University of Chinese Academy of Sciences, Beijing 100049, China
- ⁶ Sino Nitride Semiconductor Co., Ltd., Dongguan 523000, China
- * Correspondence: xinhui@semi.ac.cn (X.Z.); wxwang@iphy.ac.cn (W.W.)
- † These authors contributed equally to this work.

Abstract: This investigation explores the structural and electronic properties of low-temperature-grown $(\text{InAs})_4(\text{GaAs})_3/\text{Be}$ -doped InAlAs and InGaAs/Be-doped InAlAs multiple quantum wells (MQWs), utilizing migration-enhanced epitaxy (MEE) and conventional molecular beam epitaxy (MBE) growth mode. Through comprehensive characterization methods including transmission electron microscopy (TEM), Raman spectroscopy, atomic force microscopy (AFM), pump–probe transient reflectivity, and Hall effect measurements, the study reveals significant distinctions between the two types of MQWs. The $(\text{InAs})_4(\text{GaAs})_3/\text{Be}$ -doped InAlAs MQWs grown via the MEE mode exhibit enhanced periodicity and interface quality over the InGaAs/Be-InAlAs MQWs grown through the conventional molecule beam epitaxy (MBE) mode, as evidenced by TEM. The AFM results indicate lower surface roughness for the $(\text{InAs})_4(\text{GaAs})_3/\text{Be}$ -doped InAlAs MQWs by using the MEE mode. Raman spectroscopy reveals weaker disorder-activated modes in the $(\text{InAs})_4(\text{GaAs})_3/\text{Be}$ -doped InAlAs MQWs by using the MEE mode. This originates from utilizing the $(\text{InAs})_4(\text{GaAs})_3$ short period superlattices rather than InGaAs, which suppresses the arbitrary distribution of Ga and In atoms during the InGaAs growth. Furthermore, pump–probe transient reflectivity measurements show shorter carrier lifetimes in the $(\text{InAs})_4(\text{GaAs})_3/\text{Be}$ -doped InAlAs MQWs, attributed to a higher density of antisite defects. It is noteworthy that room temperature Hall measurements imply that the mobility of $(\text{InAs})_4(\text{GaAs})_3/\text{Be}$ -doped InAlAs MQWs grown at a low temperature of 250 °C via the MEE mode is superior to that of InGaAs/Be-doped InAlAs MQWs grown in the conventional MBE growth mode, reaching 2230 $\text{cm}^2/\text{V}\cdot\text{s}$. The reason for the higher mobility of $(\text{InAs})_4(\text{GaAs})_3/\text{Be}$ -doped InAlAs MQWs is that this short-period superlattice structure can effectively suppress alloy scattering caused by the arbitrary distribution of In and Ga atoms during the growth process of the InGaAs ternary alloy. These results exhibit the promise of the MEE growth approach for growing high-performance MQWs for advanced optoelectronic applications, notably for high-speed optoelectronic devices like THz photoconductive antennas.

Keywords: migration-enhanced epitaxial growth; low-temperature growth; InGaAs quantum well



Citation: Liu, L.; Deng, Z.; Liu, G.; Kong, C.; Du, H.; Chen, R.; Yan, J.; Qin, L.; Song, S.; Zhang, X.; et al. Low-Temperature Migration-Enhanced Epitaxial Growth of High-Quality $(\text{InAs})_4(\text{GaAs})_3/\text{Be}$ -Doped InAlAs Quantum Wells for THz Applications. *Crystals* **2024**, *14*, 421. <https://doi.org/10.3390/cryst14050421>

Academic Editors: Anelia Kakanakova and Paul J. Simmonds

Received: 14 February 2024

Revised: 25 April 2024

Accepted: 27 April 2024

Published: 29 April 2024



Copyright: © 2024 by the authors. Licensee MDPI, Basel, Switzerland. This article is an open access article distributed under the terms and conditions of the Creative Commons Attribution (CC BY) license (<https://creativecommons.org/licenses/by/4.0/>).

1. Introduction

With the increasing demand for optoelectronic devices, InGaAs quantum well (QW) technology has shown great promise for applications in fields such as photoconductive antennas (PCAs), infrared detectors, and laser diodes [1–6]. These technological advances provide new possibilities for high-performance optoelectronic conversion, which in turn drives the rapid development of terahertz (THz) technology. As a frontier science and technology with a wide range of potential applications, THz technology has demonstrated its unique value in the fields of biomedicine, materials science, drug testing, nondestructive testing, security inspection, communications technology, atmospheric science, and astronomy [7–12]. The miniaturization of core components of THz technology, including THz radiation sources and THz detectors, has become a focus of current research aimed at improving the integration and application flexibility of THz systems and reducing costs. THz PCAs fabricated from GaAs materials grown at low temperatures benefit from a simple structure, wide bandwidth and high radiation power, and can be operated at room temperature [13]. However, the use of expensive titanium-sapphire femtosecond lasers as pump sources has limited the popularity of this technology. In recent years, the development of 1.55 μm fiber femtosecond(fs) lasers to irradiate low-temperature grown InGaAs PCAs for generating and detecting THz waves has provided new possibilities for THz technology [2,14]. Compared with titanium sapphire lasers, its low price and small size can drive the development of THz radiation sources and THz detectors to the direction of cheap and integrated.

Compared to the low-temperature-grown GaAs-based THz PCAs, the radiated power from the low-temperature-grown InGaAs THz PCAs is significantly weaker, which is limited by the lower resistivity and carrier mobility of the InGaAs material itself [15]. In GaAs materials grown at low temperatures, excess As forms As antisite (As_{Ga}) defects during the growth process. These defects act as efficient nonradiative recombination and trap centers, significantly reducing the carrier lifetime. A high concentration of As antisite (As_{Ga}) defects results in the formation of As clusters (precipitates) upon annealing [16]. The formation of these precipitates causes Schottky barrier depletion around them, leading to a significant increase in resistance [16]. For low-temperature-grown InGaAs photoconductive materials, the excess As content in the material is low. Even when grown at a low temperature of 150 $^{\circ}\text{C}$, the excess As content in the InGaAs layers is only about 0.4% [17], much less than in GaAs materials grown at low temperatures ($\sim 1\text{--}2.5\%$ at ~ 200 $^{\circ}\text{C}$) [18]. This results in no significant As precipitate after annealing, and low resistivity of the annealed material. Additionally, during the low-temperature growth of InGaAs, the short migration lengths of In and Ga atoms lead to increased disorder of metal atoms in the alloy. This disorder causes alloy scattering, reducing carrier mobility [19].

Although very low carrier lifetimes (<200 fs) can be achieved with low-temperature growth of InGaAs below 200 $^{\circ}\text{C}$, the crystalline quality of the material deteriorates significantly [17,20]. Currently, the main bottlenecks in improving the performance of THz PCAs are increasing the resistivity and mobility of the low-temperature-grown InGaAs materials. In order to obtain high crystalline quality, high resistivity, and mobility in the material, InGaAs quantum wells applied to THz PCAs are typically grown above 200 $^{\circ}\text{C}$, especially 230–250 $^{\circ}\text{C}$ [2,21].

To increase the resistivity, beryllium (Be) is used for doping both the quantum well and barrier layers of InGaAs/InAlAs. However, while Be doping enhances the resistivity, it also leads to a significant reduction in carrier mobility, with mobility dropping to <600 $\text{cm}^2/\text{V}\cdot\text{s}$ (≈ 300 $\text{cm}^2/\text{V}\cdot\text{s}$ after 580 $^{\circ}\text{C}$ annealing) when Be is doped at 2×10^{18} cm^{-3} [22].

In addition to carrier scattering due to Be doping, the arbitrary distribution of In and Ga atoms during InGaAs growth causes alloy scattering, which leads to a reduction in carrier mobility [19,23]. (InAs) m (GaAs) n short-period superlattices (SPSs) consist of m monolayers (MLs) of InAs and n MLs of GaAs grown alternately. In SPSs, In and Ga atoms are distributed in an ordered arrangement within the InAs and GaAs MLs, effectively suppressing alloy scattering in InGaAs caused by the arbitrary occupancy of In and Ga

atoms in the lattice sites [19]. Therefore, the use of SPSs as an alternative to InGaAs alloys can reduce alloy scattering effects in InGaAs, which has great potential for high-speed device applications [19,24]. By employing metalorganic chemical vapor deposition (MOVPE) technology, Andre et al. grew $(\text{InAs})_n(\text{GaAs})_n$ SPSs and obtained higher carrier mobilities than InGaAs [24]. Based on these advantages of SPSs, this work will utilize $(\text{InAs})_m(\text{GaAs})_n$ SPSs to replace InGaAs alloys as the well material for quantum wells.

At low-temperature growth conditions, the migration of In and Ga adatoms on the sample surface is reduced, which is not conducive to obtaining high crystalline quality materials [25,26]. The migration-enhanced epitaxial (MEE) growth technique provides a powerful approach to achieving high-quality crystal growth at lower temperatures [27]. The MEE technique relies on alternating the supply of (In)Ga and As by opening and closing their respective shutters. Closing the shutter for As leads to a dramatic drop in its pressure, which in turn significantly extends the surface migration distance of Ga/In atoms, even when the substrate is kept at a relatively low temperature. High-quality crystalline quantum well structures are crucial for the creation of optoelectronic devices with enhanced performance. Due to these significant advantages, the MEE method has emerged as a promising approach for growing III-V compound materials at low temperatures [23,24,26–29].

The primary difference between MEE and conventional MBE growth modes is their growth mechanisms. The MEE mode enhances the mobility of atoms on the substrate by alternately supplying the growth atoms, instead of supplying them all at once. This method facilitates the atoms in finding the lowest energy positions on the substrate surface, leading to the formation of smoother interfaces and higher quality materials. In contrast, the conventional MBE mode supplies all atoms simultaneously, which may result in atoms being fixed at non-ideal positions before finding the optimal locations, thereby increasing surface roughness and defects.

Gerard et al. employed the MEE growth mode to grow $(\text{InAs})_4(\text{GaAs})_3$ SPSs with a thickness of 130 nm on InP (100) substrates at 370 °C. Scanning transmission electron microscopy characterization showed that the material is lattice-matched, exhibits good crystalline quality, and does not show significant misfit dislocations [27]. In further studies of the $(\text{InAs})_4(\text{GaAs})_3$ SPSs, Gerard et al. found that its actual bandgap is about 0.76 eV [30], which is in close proximity to the 0.743 eV bandgap exhibited by $\text{In}_{0.53}\text{Ga}_{0.47}\text{As}$ at room temperature. Using the MEE growth mode to grow $(\text{InAs})_4(\text{GaAs})_3$ SPSs as the well material in quantum well instead of InGaAs can suppress the alloy scattering caused by the arbitrary distribution of In and Ga throughout the growth of InGaAs, achieving the growth of high-quality quantum wells at low temperatures [30].

From the research of Gerard et al., it is evident that they successfully grew high-quality $(\text{InAs})_4(\text{GaAs})_3$ SPSs with a thickness of 130 nm on InP (100) substrates at a low temperature of 370 °C [27]. In order to achieve a good lattice match with the InP (100) substrate and to maintain an integer number of atomic layers for both InAs and GaAs, the same number of atomic layers as in the work of Gerard et al. were used in this study. However, the purpose of this study is to grow materials for THz photoconductive antennas, and thus the material structure differs from that of Gerard et al. The structure grown in this work consists of 12 nm $(\text{InAs})_4(\text{GaAs})_3$ /12 nm Be-doped InAlAs multiple quantum wells (MQWs) with a periodicity of 50 cycles. To achieve high mobility and resistivity, this study employs the growth of $(\text{InAs})_4(\text{GaAs})_3$ /Be-doped InAlAs multiple quantum wells (MQWs) at low temperatures using the MEE growth mode, as an alternative to the traditional InGaAs/InAlAs quantum wells. In addition to testing the crystal quality of the materials, this paper also characterizes important parameters for THz photoconductive antennas, such as carrier lifetime and mobility. The low growth temperature of 250 °C (thermocouple temperature) was used to reduce the carrier lifetime. Beryllium doping the InAlAs quantum well barriers was introduced to increase resistivity. The MQWs utilized 12 nm thick $(\text{InAs})_4(\text{GaAs})_3$ SPSs as wells, replacing $\text{In}_{0.53}\text{Ga}_{0.47}\text{As}$ as the femtosecond laser absorption layer for THz photoconductive antennas, suppressing alloy scattering and enhancing mobility. Moreover, the MEE growth mode was used to independently control

the opening time of the As shutter, increasing the excess As content to further reduce the carrier lifetime, which helps to increase the resistivity after subsequent annealing.

We have conducted some preliminary research on the low-temperature growth of MQWs using the MEE mode [11]. The sample structure in this study differs from that in our previous works. In this work, only the InAlAs barriers were doped, while the wells themselves were not doped. The absence of Be doping in the wells can reduce impurity scattering, which is beneficial for enhancing electron mobility. This study introduced atomic force microscopy (AFM) measurements, which provided more comprehensive information about the samples and helped us to gain a deeper understanding of the sample properties. Additionally, this paper investigated the Raman spectra of annealed samples and observed the influence of stress on the Raman spectra before and after annealing.

2. Materials and Methods

The samples investigated in this research were grown by employing the FW-VI-60 type Molecular Beam Epitaxy (MBE), produced by SKY Technology Development Co., Ltd., Shenyang, China. The growth of all samples was carried out on a quarter of a 2-inch semi-insulating IP (100) substrate. The structure of sample A contained 50 periods of quantum wells, each period consisting of a 12 nm thick $\text{In}_{0.52}\text{Al}_{0.48}\text{As}$ layer as the barrier and a 12 nm thick $(\text{InAs})_4(\text{GaAs})_3$ layer as the well. The $(\text{InAs})_4(\text{GaAs})_3$ layer was grown utilizing the MEE mode, characterized by the alternate switching In (or Ga) and As shutters throughout the growth of InAs or GaAs layers. In contrast, the structure of sample B also included 50 periods of quantum wells but was grown by using the conventional MBE mode, with a 12 nm thick layer of $\text{In}_{0.53}\text{Ga}_{0.47}\text{As}$ as the well region and a 12 nm thick layer of $\text{In}_{0.52}\text{Al}_{0.48}\text{As}$ as the barrier region. Both samples A and B had the $\text{In}_{0.52}\text{Al}_{0.48}\text{As}$ layer doped with Be at a concentration of $2 \times 10^{18} \text{ cm}^{-3}$. The epitaxial growth of samples A and B was carried out at a thermocouple-measured temperature of 250 °C, as measured by a thermocouple. Prior to growth, the 1/4 of a 2-inch semi-insulating InP (100) substrate was maintained at 550 °C (thermocouple temperature) under As protection for 5 min to remove the oxide layer.

The grown samples were analyzed for crystalline quality using the high angle annular dark field scanning transmission electron microscopy (HAADF-STEM), bright-field scanning transmission electron microscopy (BF-STEM), and high-resolution transmission electron microscopy (HRTEM) techniques. The instrument used is the Thermofisher Talos F200X (Waltham, MA, USA). To perform the HAADF-STEM cross-sectional observation, the required samples were first prepared using focused ion beam (FIB) technology. In this research, the examination of the sample surfaces was conducted through atomic force microscopy (AFM) utilizing a Bruker Dimension ICON system (Bruker, Billerica, MA, USA), operating in tapping mode.

In addition, the electrical parameters of the samples such as mobility and resistivity were determined by Hall effect measurements using the HL5500 system from Nanometrics Incorporated (Milpitas, CA, USA). Moreover, the lifetime of carriers in the samples was measured at room temperature, employing the pump-probe transient reflectivity technique ($\Delta R/R$) for characterization. In order to achieve this purpose, this study utilized a titanium-sapphire regenerative amplifier (Legend Elite, Coherent Inc., Sunnyvale, CA, USA) to pump an optical parametric amplifier (OPA, Opera Solo, Coherent Inc., Sunnyvale, CA, USA). In this paper, the pulse width of the OPA output was approximately 150 fs, with a 1 kHz operational repetition frequency. The pump and probe beams were both linearly polarized, and their wavelength was adjusted to be in close proximity to the quantum well's bandgap, which was around 1.45 μm .

In this study, micro-Raman spectra of the quantum well samples at room temperature were acquired using Horiba's LabRAM HR Evolution. The excitation wavelength was fixed at 532 nm, utilizing an excitation power of 2.280 mW, which was quantified using a Thorlabs S130C power meter (Thorlabs, Newton, NJ, USA).

3. Results and Discussions

3.1. TEM Characterization of $(\text{InAs})_4(\text{GaAs})_3/\text{Be-Doped InAlAs}$ MQWs Grown at Low Temperatures by Using the MEE Growth Mode

This study characterized sample A using BF-STEM, HAADF-STEM, and HRTEM techniques, with results shown in Figure 1a, b, and c, respectively. The BF-STEM and HAADF-STEM results show that the quantum well and barrier widths in sample A were 12 nm, consistent with the design values. The quantum wells exhibited significant periodicity and steep interfaces. Notably, the $(\text{InAs})_4(\text{GaAs})_3$ SPS as the potential well had a pronounced periodicity with steep interfaces, displayed strong periodicity and abrupt interfaces, with a structure consisting of four InAs monolayers and three GaAs monolayers grown alternately. These results are similar to the STEM results of the 130 nm thick $(\text{InAs})_4(\text{GaAs})_3$ SPS grown by Gerard et al. at 370 °C [27]. The difference in this study is that the $(\text{InAs})_4(\text{GaAs})_3$ SPS was grown at a significantly lower temperature (250 °C) and was used as a potential well with 50 cycles. The total thickness of the $(\text{InAs})_4(\text{GaAs})_3$ SPS in Sample A reached 600 nm, exhibiting high crystalline quality. The HRTEM results (Figure 1c) further confirm the good crystallinity, the absence of discernible misfit dislocations or defects, and the pronounced periodicity of the $(\text{InAs})_4(\text{GaAs})_3$ superlattice, rather than a random InGaAs alloy.

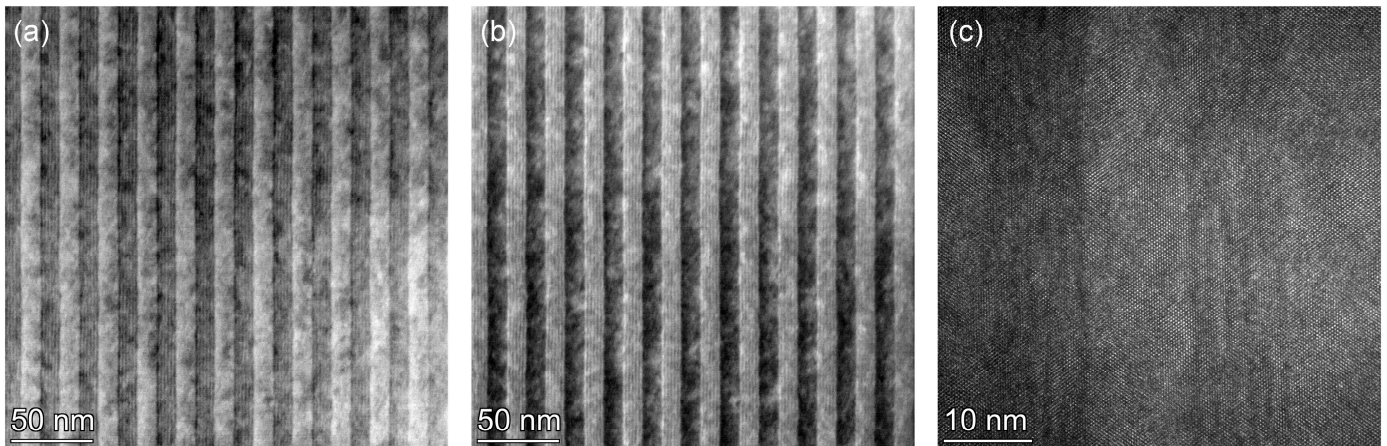


Figure 1. TEM images of sample A, a low-temperature grown 12 nm $(\text{InAs})_4(\text{GaAs})_3/12$ nm Be-doped InAlAs MQWs: (a) BF-STEM image; (b) HAADF-STEM image; (c) HRTEM image.

3.2. TEM Characterization of $\text{InGaAs}/\text{Be-Doped InAlAs}$ MQWs Grown at Low Temperatures by Using the Conventional MBE Growth Mode

This study characterized sample B using BF-TEM, HAADF-STEM, and HRTEM techniques, with the results presented in Figure 2a,b, and c, respectively. Sample B consisted of 12 nm InGaAs/12 nm Be-doped InAlAs MQWs grown by conventional MBE mode at a substrate temperature of 250 °C (thermocouple temperature). The BF-TEM and HAADF-STEM results (Figure 2a,b) showed that the quantum well interfaces of sample B were abrupt with a distinct periodicity. The HRTEM results (Figure 2c) further demonstrate that sample B had good crystalline quality without observable misfit dislocations and defects. In contrast to sample A shown in Figure 1, for sample B no multilayer structure was found in the quantum well region. This can be ascribed to the conventional MBE growth mode used for sample B, where the InGaAs layers were not grown in an atomic layer-by-layer manner using the MEE mode.

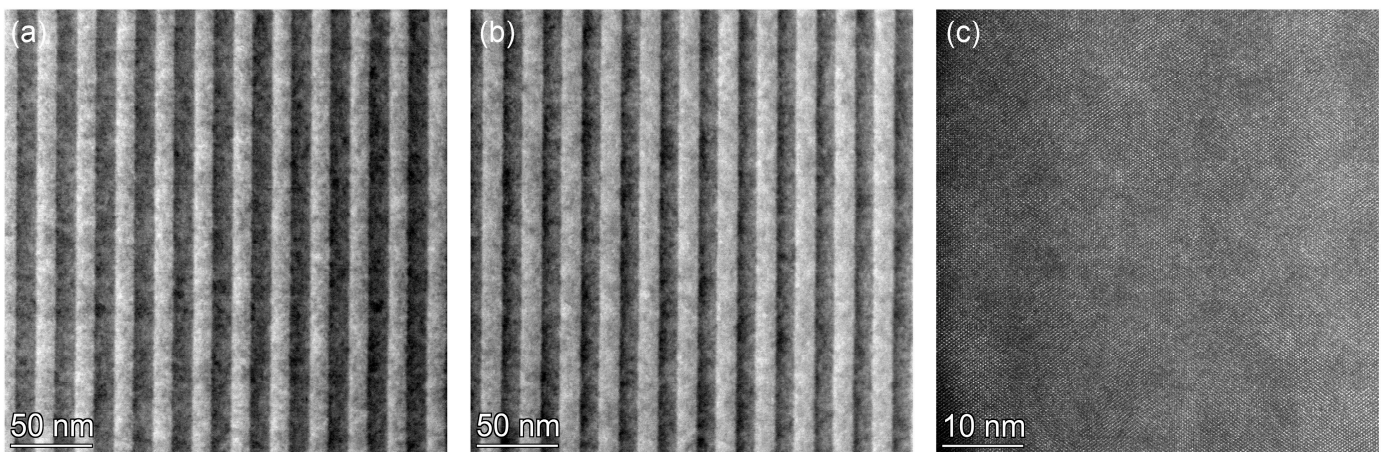


Figure 2. TEM images of sample B, a low-temperature grown 12 nm InGaAs/12 nm Be-doped InAlAs MQWs: (a) BF-STEM image; (b) HAADF-STEM image; (c) HRTEM image.

3.3. AFM Images of Low-Temperature-Grown $(\text{InAs})_4(\text{GaAs})_3/\text{Be-Doped InAlAs}$ and InGaAs/Be-Doped InAlAs MQWs

Figure 3 shows the two-dimensional AFM images obtained by tapping mode imaging of low-temperature grown 12 nm $(\text{InAs})_4(\text{GaAs})_3/12$ nm Be-doped InAlAs MQWs and 12 nm InGaAs/12 nm Be-doped InAlAs MQWs, with a scanning range of $1 \times 1 \mu\text{m}$. As can be seen from the figure, the surfaces of the epitaxial films of both $(\text{InAs})_4(\text{GaAs})_3/\text{Be-doped InAlAs}$ MQWs and InGaAs/Be-doped InAlAs MQWs samples are remarkably smooth, with root-mean-square roughness (R_q) values of 0.271 and 0.324 nm, respectively. The R_q of $(\text{InAs})_4(\text{GaAs})_3/\text{Be-doped InAlAs}$ MQWs, which were grown using the MEE mode, was lower than that of InGaAs/Be-doped InAlAs MQWs. This difference can be ascribed to the precise atomic layer-by-layer deposition of $(\text{InAs})_4(\text{GaAs})_3/\text{Be-doped InAlAs}$ MQWs, enabled by the MEE mode. This method enhances the migration of group III adatoms on the surface, resulting in a smoother sample surface.

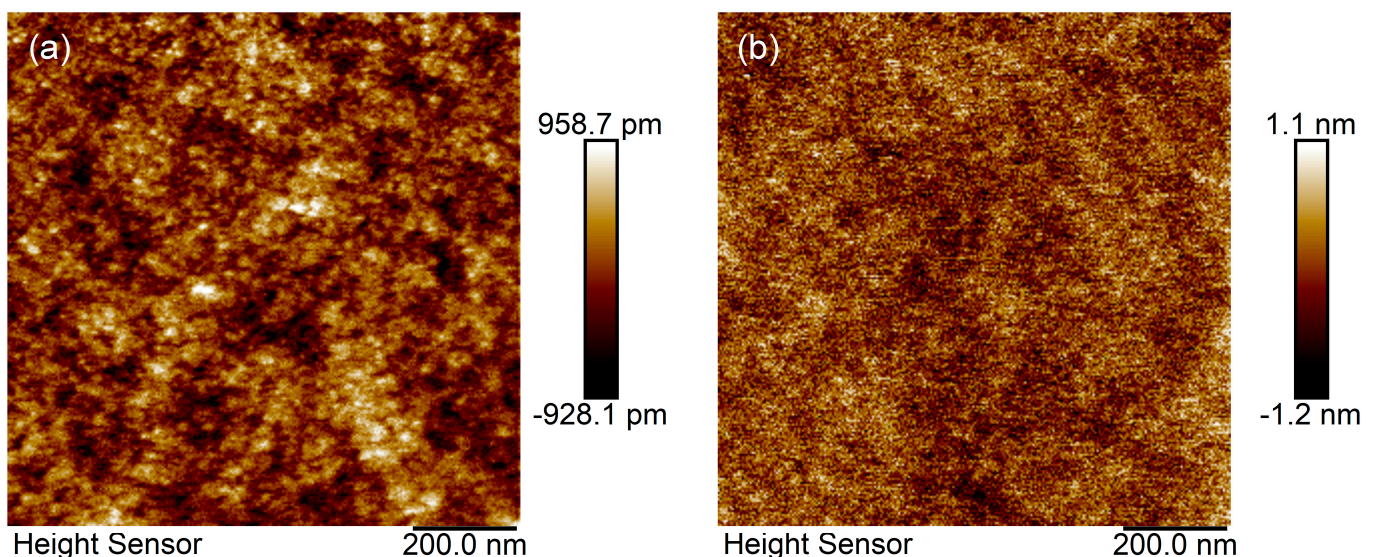


Figure 3. AFM images of low temperature-grown MQWs with a scanning range of $1 \times 1 \mu\text{m}$: (a) 12 nm $(\text{InAs})_4(\text{GaAs})_3/12$ nm Be-doped InAlAs MQWs; (b) 12 nm InGaAs/12 nm Be-doped InAlAs MQWs.

3.4. Raman Characterization of $(\text{InAs})_4(\text{GaAs})_3/\text{Be-Doped InAlAs}$ and InGaAs/Be-Doped InAlAs MQWs Grown at Low Temperatures

Raman spectroscopy plays a key role in the characterization of semiconductor materials, in particular quantum wells and superlattice structures [31,32]. It is uniquely suited

to reveal the quality of crystallization within a material and to assess the quality of the interface. In this study, we performed a detailed analysis of multiple quantum well samples in two different growth modes by Raman spectroscopy to obtain important information about the periodicity of the material and the quality of the interface. For sample A (12 nm $(\text{InAs})_4(\text{GaAs})_3/12$ nm Be-doped InAlAs MQWs) and sample B (12 nm InGaAs/12 nm Be-doped InAlAs MQWs), their Raman spectra at room temperature exhibited different peaks (Figure 4).

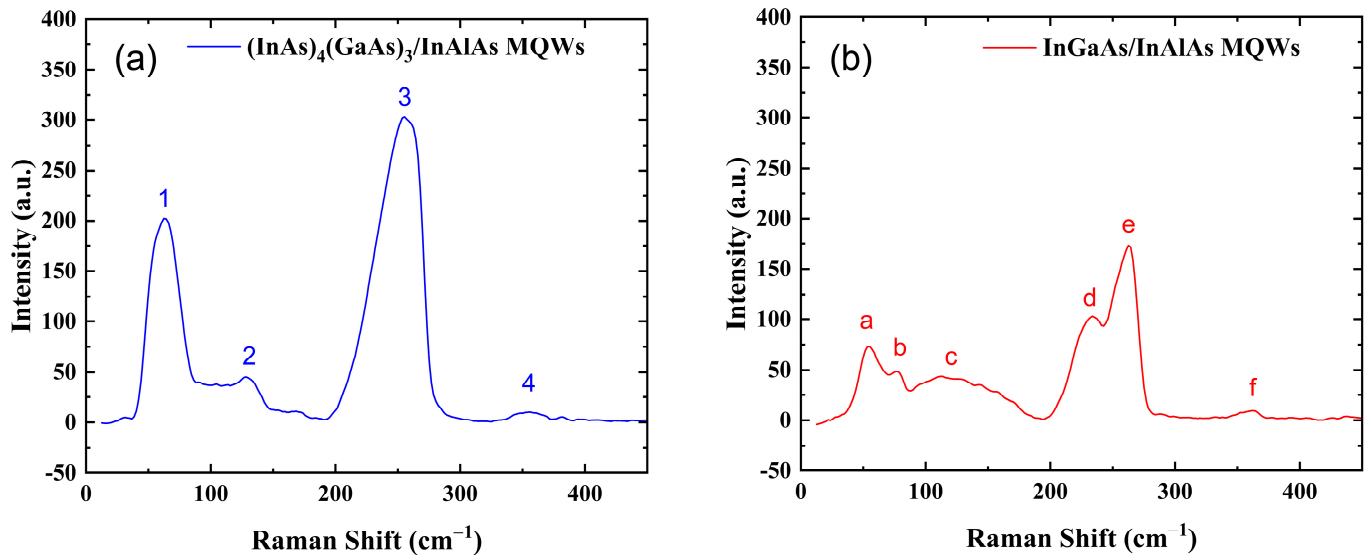


Figure 4. Raman spectra of MQWs grown at low temperatures: (a) $(\text{InAs})_4(\text{GaAs})_3/\text{Be-doped InAlAs}$ MQWs; and (b) InGaAs/Be-doped InAlAs MQWs.

The longitudinal acoustic (LA) modes observed at the Brillouin zone center revealed critical information about the periodic arrangement of superlattices [31]. The vibrational bands corresponding to these modes reflect low-frequency vibrations between atoms or molecules within the material, typically observed at wavenumbers ranging from 10 to 100 cm^{-1} . Analysis of the LA modes enables observation of low-frequency acoustic vibrations among distinct atomic layers within superlattices or quantum wells, manifested primarily as longitudinal compression and stretching along the growth direction lattice. For MQWs or superlattice structures, the vibrational characteristics of longitudinal acoustic modes can indicate the orderliness and periodic changes in the atomic arrangement at the interface, providing an important perspective for investigating superlattices or quantum wells. The peak labeled as “1” in the Raman spectrum of Figure 4a is attributed to the longitudinal acoustic mode, which is highly correlated with the periodic structure of the superlattice. The location of this peak is near the longitudinal acoustic mode position of the $(\text{InAs})_4(\text{GaAs})_3$ superlattice as reported in reference [33], and its position can be calculated by the formulas in literature [34]. This peak was not detected in sample B, indicating that the quantum well regions of sample A have different lattice vibration modes compared to the quantum well regions of sample B.

Sample B’s Raman spectrum exhibited a noticeable peak at around 52 cm^{-1} , assigned the label ‘a’, which is recognized as a distinctive feature of the transverse acoustic (TA) phonon mode intrinsic to InAs. This TA mode depicts the vibrations of the In and As atoms along an axis perpendicular to the direction of propagation of the lattice vibrations. The TA mode Raman peak of InAs was not observed in Sample A, possibly due to two reasons. Firstly, the InAs in the $(\text{InAs})_4(\text{GaAs})_3$ SPS is subjected to compressive stress, leading to an increase in Raman shift. Secondly, the $(\text{InAs})_4(\text{GaAs})_3$ SPS grown by MEE exhibits excellent periodicity, which enhances the intensity of its Raman peaks. This enhanced intensity

may cause the TA mode Raman peak of InAs to merge with the nearby LA peak of the $(\text{InAs})_4(\text{GaAs})_3$ SPS.

The appearance of the disorder-activated longitudinal acoustic (DALA) mode peaks in the Raman spectra of samples A and B significantly indicates the presence of disorder within the materials. Samples A and B exhibit Raman peaks designated as '2', 'b', and 'c', which are ascribed to DALA modes, a finding that is supported by references in the literature [35,36]. The molecular vibrational bands characteristic of the DALA modes correspond to atomic vibrations parallel to the direction of wave propagation, although these vibrations are affected by structural disorders. The appearance and strength of DALA peaks within Raman spectra are directly linked to the level of disorder. The reduced intensity of DALA peaks in sample A in contrast to sample B indicates that the $(\text{InAs})_4(\text{GaAs})_3/\text{Be}$ -doped InAlAs MQWs grown by using the MEE mode exhibit enhanced atomic arrangement compared to the InGaAs/Be-doped InAlAs MQWs grown by using the conventional MBE mode. This suggests MEE as a potent method to realize MQW structures with highly ordered atomic organization. Such atomic-level disorder in InGaAs/InAlAs MQWs grown in a conventional MBE mode at low temperatures may adversely affect the carrier mobility of the material.

Longitudinal optical (LO) phonon modes refer to the movements of atoms in the lattice that occur parallel to the path of phonon propagation. In the Raman spectrum of sample A, a pronounced peak was detected at a wavenumber of 255 cm^{-1} (denoted as '3') [33,37], which is attributed to the coalescence of LO phonon modes originating from both InAs and GaAs compounds. This overlap is attributed to the compressive strain in the InAs layer and the tensile strain in the GaAs layer, causing their Raman peaks to shift towards each other and eventually merge at 255 cm^{-1} . This result highlights the significant effect of strain on the LO phonon modes in strained-layer superlattices. In contrast, the Raman peaks in sample B show that the LO modes of InAs and GaAs are located at 233 cm^{-1} (labeled as 'd') and 263 cm^{-1} (labeled as 'e'), respectively, which is consistent with literature reports [38].

In the case of samples A and B, peaks detected through Raman spectroscopy near 360 cm^{-1} (identified as '4' and 'f'), representing the relative LO phonon, involving the relative motion between aluminum and arsenic atoms along the direction of phonon propagation. This is consistent with previous studies [36,37].

Raman spectroscopy analysis of samples A and B confirms that the $(\text{InAs})_4(\text{GaAs})_3/\text{Be}$ -doped InAlAs multi-quantum wells grown by the MEE technique possess remarkable periodicity. This periodic structure effectively suppresses alloy scattering inside the quantum wells. The TEM results also confirm the realization of a well-ordered periodic structure through the utilization of the MEE mode. Although the interfaces of low-temperature grown InGaAs/InAlAs quantum wells are very sharp, Raman spectroscopy detects significant chaos in the positioning of group III atoms inside the quantum wells, resulting in considerable alloy scattering. Therefore, Raman spectroscopy can effectively assess the crystal quality of quantum wells grown at low temperatures, complementing the TEM results.

To investigate the relationship between stress and Raman peak, the following procedure was used in this study. First, the sample was rapidly annealed for 10 min in a hydrogen atmosphere at a temperature of $580\text{ }^\circ\text{C}$. To protect the sample during high-temperature annealing, the sample surface was covered with a GaAs substrate.

By comparing the Raman spectroscopy data in Figures 4 and 5, we observed significant differences in the spectral response of $(\text{InAs})_4(\text{GaAs})_3/\text{Be}$ -doped InAlAs MQWs and InGaAs/Be-doped InAlAs MQWs samples before and after high-temperature annealing. For the $(\text{InAs})_4(\text{GaAs})_3/\text{Be}$ -doped InAlAs MQWs, the high-temperature annealing treatment led to noticeable changes in the position of the Raman peaks, indicating that the annealing process induced a significant alteration in the internal stress state of the sample. In contrast, the Raman spectra of the InGaAs/Be-doped InAlAs MQWs sample did not exhibit significant changes before and after annealing, suggesting that its internal stress state was less affected by the annealing process.

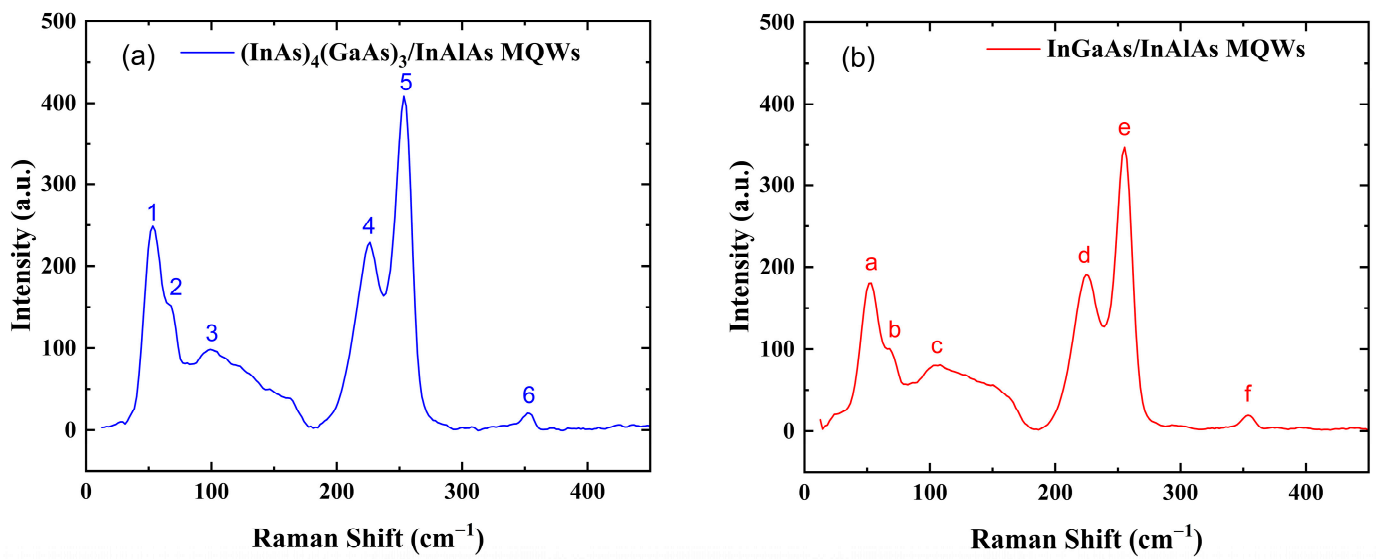


Figure 5. Raman spectra of low-temperature-grown MQWs after annealing: (a) $(\text{InAs})_4(\text{GaAs})_3/\text{Be}$ -doped InAlAs MQWs; and (b) InGaAs/Be-doped InAlAs MQWs.

In the Raman spectrum of the $(\text{InAs})_4(\text{GaAs})_3/\text{Be}$ -doped InAlAs MQWs sample, the peak labeled as 1, located at 52 cm^{-1} , corresponds to the TA phonon mode of InAs. Prior to high-temperature annealing, the Raman peaks labeled as 1 and 2 were merged due to the influence of internal stress in the sample, resulting in a broadened peak. However, after the high-temperature annealing treatment, these two Raman peaks separated, corresponding to the TA mode of InAs and the LA mode of the $(\text{InAs})_4(\text{GaAs})_3$ SPS, respectively. This phenomenon indicates that the high-temperature annealing process effectively released the internal stress within the quantum wells. By analyzing the changes in peak positions in the Raman spectra, we can obtain crucial information about the internal stress state of the material, providing guidance for optimizing the growth and thermal treatment processes of multiple quantum well structures.

In Figure 5a, the Raman peak labeled as 3 corresponds to the DALA mode, indicating the presence of disorder in the material. Compared to the unannealed sample in Figure 4a, the intensity of the Raman peak labeled as 3 increased after high-temperature annealing. This phenomenon suggests that during the high-temperature annealing process, atomic disorder increases while internal stresses in the sample are released. Furthermore, the LO modes of InAs and GaAs, labeled as 4 and 5 in Figure 5a, separated after high-temperature annealing compared to their state before annealing. This change is also attributed to the release of internal stress during the high-temperature annealing process.

3.5. Carrier Lifetime and Hall Effect of $(\text{InAs})_4(\text{GaAs})_3/\text{Be}$ -Doped InAlAs and InGaAs/Be-Doped InAlAs MQWs Grown at Low Temperatures

This study utilized pump–probe transient reflectivity measurements to characterize the carrier dynamics within $(\text{InAs})_4(\text{GaAs})_3/\text{Be}$ -doped InAlAs and InGaAs/Be-doped InAlAs MQWs grown at low temperatures. The experiments were performed at room temperature, using a pump wavelength set to 1450 nm and a pump power tuned to 6 mW. Figure 6a,b show the decay traces of transient reflectivity over time for both MQWs samples. By curve fitting, the carrier lifetimes of 12 nm $(\text{InAs})_4(\text{GaAs})_3/\text{Be}$ -doped InAlAs and 12 nm InGaAs/Be-doped InAlAs MQWs were obtained as 4.57 ps and 7.97 ps, respectively. Compared to the carrier lifetime of approximately 7.8 ps for Be-doped InGaAs material grown at low temperature ($250\text{ }^\circ\text{C}$) reported in the literature [39], the lifetime in InGaAs/Be-doped InAlAs MQWs from this work is comparable. However, the $(\text{InAs})_4(\text{GaAs})_3/\text{InAlAs}$ MQWs exhibited a shorter lifetime, which could be due to the slower growth rate and longer arsenic supply duration in the MEE growth causing an increased density of antisite defects (As_{Ga}) where As substitutes Ga sites in the MQWs. These antisite defects act as non-

radiative recombination centers, reducing the carrier lifetime. For low-temperature-grown materials, it has been reported in the literature that an increase in the density of antisite defects leads to a decrease in the carrier lifetime [40].

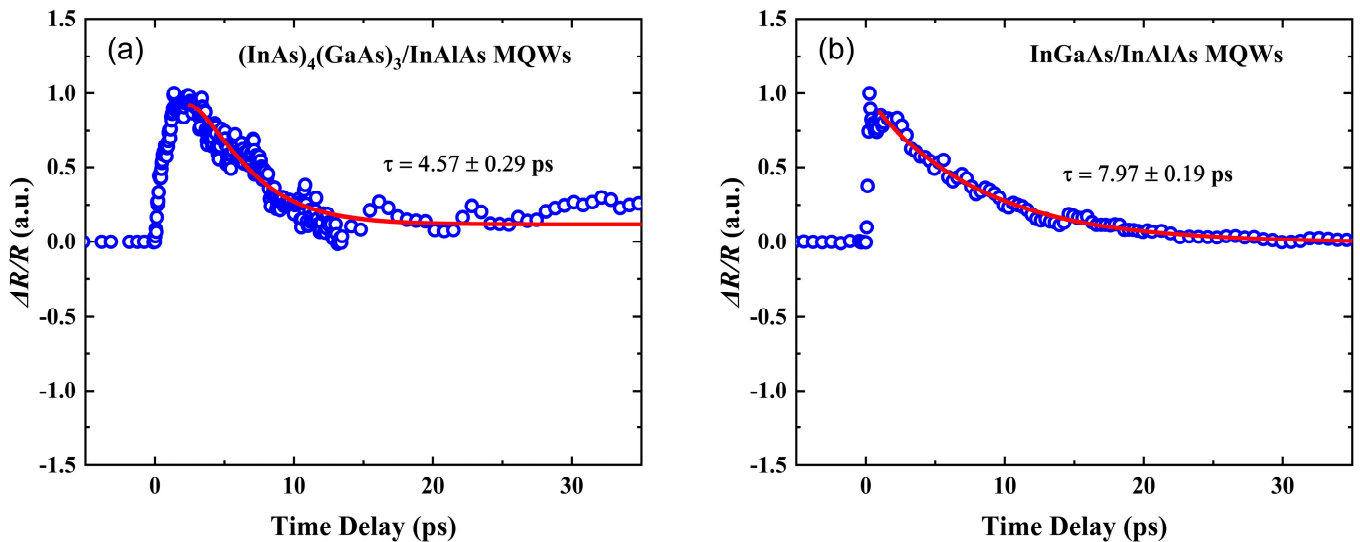


Figure 6. Transient reflectivity analysis using pump–probe techniques of low-temperature-grown MQWs with a pump wavelength of 1450 nm at room temperature. The scattered blue circles show the experimentally obtained data, while the approximation through fits to a single exponential decay function is shown with red solid lines for two types of MQWs: (a) (InAs)₄(GaAs)₃/Be-doped InAlAs MQWs; (b) InGaAs/Be-doped InAlAs MQWs.

In the development of high-speed optoelectronic devices, such as THz photoconductive antennas, the mobility and carrier lifetime of the material play a crucial role in determining the performance. To assess these electrical properties, this study conducted room temperature Hall effect measurements on low-temperature-grown (InAs)₄(GaAs)₃/Be-doped InAlAs MQWs by using MEE mode, and low-temperature-grown InGaAs/Be-doped InAlAs MQWs by using the conventional MBE mode, respectively. The results show that the (InAs)₄(GaAs)₃/Be-doped InAlAs MQWs grown under the MEE growth mode exhibited an electron mobility of 2230 cm²/V.s, while the InGaAs/Be-doped InAlAs MQWs grown under the conventional MBE growth mode exhibited an electron mobility reaching 1900 cm²/V.s. In contrast, a previous study reported that InGaAs materials doped with Be at a low growth temperature of 250 °C exhibited a room temperature mobility of only around 200 cm²/V.s (at a Be doping concentration of 2×10^{18} cm⁻³) [39].

The main challenge in controlling the distribution of In and Ga atoms during the growth of InGaAs is the random occupation of group III atomic sites by In and Ga atoms. This random distribution leads to a situation where In atoms occupy Ga sites and vice versa, leading to alloy scattering within the InGaAs material. Alloy scattering reduces the carrier mobility, which is difficult to overcome only by adjusting the growth process conditions.

To address this challenge, a short-period superlattice structure of (InAs)₄(GaAs)₃ can be used as an alternative to InGaAs. In this approach, the InAs and GaAs layers are grown alternately during the growth process, with an effective In composition similar to that of InGaAs. By using this structure, the random distribution of In and Ga atoms and the resulting alloy scattering can be avoided. The superlattice structure allows for a more controlled distribution of In and Ga atoms, as they are confined to their respective layers during growth. The findings of this study on (InAs)₄(GaAs)₃/Be-doped InAlAs MQWs grown via MEE contribute to the advancement of high-speed optoelectronic devices by demonstrating enhanced carrier mobility and shorter carrier lifetimes. This result provides valuable insights into the material design of high-performance optoelectronic devices, especially for high-performance THz photoconductive antennas.

4. Conclusions and Perspectives

Our study demonstrates that the growth mode has a significant impact on the structural and electronic properties of low-temperature-grown MQWs. Specifically, the $(\text{InAs})_4(\text{GaAs})_3/\text{Be-doped InAlAs}$ MQWs grown through the MEE growth mode present better structural periodicity, smoother surfaces, and lower disorder compared to their $\text{InGaAs}/\text{InAlAs}$ counterparts grown by the conventional MBE mode. These improvements are crucial as they lead to a significant enhancement of carrier mobility and suggest the potential for superior optoelectronic performance, which is essential for deployment in high-speed optoelectronic devices including THz photoconductive antennas. The better performance of $(\text{InAs})_4(\text{GaAs})_3/\text{Be-doped InAlAs}$ MQWs is attributed to the adoption of a short-period superlattice structure. This structure effectively reduces alloy scattering, which is a common issue when In and Ga atoms are randomly distributed during the growth of the InGaAs ternary alloy. However, it is important to note that the $(\text{InAs})_4(\text{GaAs})_3/\text{Be-doped InAlAs}$ MQWs grown at low temperatures using the MEE growth method exhibited shorter lifetimes, a consequence of slower growth rates and extended arsenic supply during the MEE growth process, leading to an increased presence of antisite defects (As_{Ga}). These defects serve as centers for non-radiative recombination, reducing the carrier lifetime.

In summary, our study highlights the importance of selecting the appropriate growth mode when fabricating MQWs. $(\text{InAs})_4(\text{GaAs})_3/\text{Be-doped InAlAs}$ MQWs grown at low temperatures through the MEE growth method exhibit superior structural and electronic qualities that enable high carrier mobility and potential for enhanced optoelectronic performance. Future work should focus on optimizing the growth parameters to meet the needs of specific applications, while also delving into interface phenomena and defect formation mechanisms for a deeper fundamental understanding. For device applications, the range of applications can be extended, such as the application of grown materials to ultrafast photodetectors, high-speed transistors, and other fields. This study employed the MEE method for low-temperature growth of $(\text{InAs})_4(\text{GaAs})_3/\text{Be-doped InAlAs}$ MQWs, achieving high crystal quality and periodic MQWs, while suppressing alloy scattering in low-temperature-grown InGaAs MQWs. This research demonstrates the potential of optimized MQWs in optoelectronic devices, providing new insights for advancing epitaxial growth techniques and innovative applications in high-speed optoelectronic devices. The principles and optimization strategies employed in this study can be potentially extended to various material systems beyond $(\text{InAs})_4(\text{GaAs})_3/\text{InAlAs}$ and $\text{InGaAs}/\text{InAlAs}$ MQWs, opening up new avenues for the application of high-quality epitaxial layers in diverse optoelectronic devices across different material systems.

In the process of growing complex nanostructured quantum materials, the role of density functional theory (DFT) simulations is becoming increasingly important. DFT simulations can provide vital information on the electronic properties of materials and intermolecular interactions, which are crucial for understanding and optimizing material growth processes [41]. Therefore, we suggest that future studies should include DFT simulations to comprehensively understand the growth behavior of materials by combining experimental results and theoretical simulations, which can guide experimental design and optimize material properties.

Author Contributions: Conceptualization, L.L.; Methodology, W.W., X.Z. and L.L.; Samples growth, L.L., L.Q., W.W. and Z.D.; characterization, L.L., G.L., C.K., R.C., J.Y., H.D. and X.Z.; formal analysis, L.L., G.L., X.Z. and W.W.; resources, W.W. and S.S.; supervision, W.W. and L.L.; writing—original draft preparation, L.L.; writing—review and editing, X.Z. and L.L.; visualization, L.L., C.K. and X.Z.; project administration, L.L., X.Z. and S.S.; funding acquisition, L.L. and X.Z. All authors have read and agreed to the published version of the manuscript.

Funding: This research was funded by the National Natural Science Foundation of China (No. 61964003), the Science and Technology Base and Talent Special Project of Guangxi (No. GuiKeAD20238095), Guilin Innovation Platform and Talent Plan (No. 20210217-9), the Strategic Priority Research Program of

Chinese Academy of Sciences (No. XDB43000000) and the University-Enterprise Cooperation Program of School of Electronic Information and Modern Industry, Guangxi Normal University.

Data Availability Statement: The original contributions presented in the study are included in the article, further inquiries can be directed to the corresponding authors.

Conflicts of Interest: Author Jianfeng Yan was employed by the company Sino Nitride Semiconductor Co., Ltd. The remaining authors declare that the research was conducted in the absence of any commercial or financial relationships that could be construed as potential conflicts of interest.

References

- Dietz, R.J.B.; Globisch, B.; Gerhard, M.; Velauthapillai, A.; Stanze, D.; Roehle, H.; Koch, M.; Göbel, T.; Schell, M. 64 μ W Pulsed Terahertz Emission from Growth Optimized InGaAs/InAlAs Heterostructures with Separated Photoconductive and Trapping Regions. *Appl. Phys. Lett.* **2013**, *103*, 061103. [[CrossRef](#)]
- Dai, D.; Liu, H.; Su, X.; Shang, X.; Li, S.; Ni, H.; Niu, Z. High Resistivity and High Mobility in Localized Beryllium-Doped InAlAs/InGaAs Superlattices Grown at Low Temperature. *Crystals* **2023**, *13*, 1417. [[CrossRef](#)]
- Takazato, A.; Kamakura, M.; Matsui, T.; Kitagawa, J.; Kadoya, Y.Y. Terahertz Wave Emission and Detection Using Photoconductive Antennas Made on Low-Temperature-Grown InGaAs with 1.56 μ m Pulse Excitation. *Appl. Phys. Lett.* **2007**, *91*, 011102. [[CrossRef](#)]
- Riyaj, M.; Rathi, A.; Singh, A.K.; Pushpalata; Alvi, P. A. Bandgap Tailoring and Optical Response of InAlAs/InGaAs/GaAsSb Double Quantum Well Heterostructures: The Impact of Uniaxial Strain and Well Width Variations. *J. Mod. Opt.* **2022**, *69*, 1229–1238. [[CrossRef](#)]
- Peng, Z. Taro Arakawa Tunable Vernier Series-Coupled Microring Resonator Filters Based on InGaAs/InAlAs Multiple Quantum-Well Waveguide. *Photonics* **2023**, *10*, 1256. [[CrossRef](#)]
- Liu, Z.; Liu, H.; Jiang, C.; Ma, B.; Wang, J.; Ming, R.; Liu, S.; Ge, Q.; Ren, R.; Lin, J.; et al. Improved Performance of InGaAs/AlGaAs Quantum Well Lasers on Silicon Using InAlAs Trapping Layers. *Opt. Express* **2023**, *31*, 7900. [[CrossRef](#)]
- Bacon, D.R.; Madéo, J.; Dani, K.M. Photoconductive Emitters for Pulsed Terahertz Generation. *J. Opt.* **2021**, *23*, 064001. [[CrossRef](#)]
- Yachmenev, A.E.; Khabibullin, R.A.; Ponomarev, D.S. Recent Advances in THz Detectors Based on Semiconductor Structures with Quantum Confinement: A Review. *J. Phys. D* **2022**, *55*, 193001. [[CrossRef](#)]
- Muttlak, S.G.; Abdulwahid, O.S.; Sexton, J.; Kelly, M.J.; Missous, M. InGaAs/AlAs Resonant Tunneling Diodes for THz Applications: An Experimental Investigation. *IEEE J. Electron. Devices Soc.* **2018**, *6*, 254–262. [[CrossRef](#)]
- Yardimci, N.T.; Cakmakyapan, S.; Hemmati, S.; Jarrahi, M. A High-Power Broadband Terahertz Source Enabled by Three-Dimensional Light Confinement in a Plasmonic Nanocavity. *Sci. Rep.* **2017**, *7*, 4166. [[CrossRef](#)] [[PubMed](#)]
- Liu, L.; Chen, R.; Kong, C.; Deng, Z.; Liu, G.; Yan, J.; Qin, L.; Du, H.; Song, S.; Zhang, X.; et al. Low-Temperature Growth of InGaAs Quantum Wells Using Migration-Enhanced Epitaxy. *Materials* **2024**, *17*, 845. [[CrossRef](#)] [[PubMed](#)]
- Chen, R.; Li, X.; Du, H.; Yan, J.; Kong, C.; Liu, G.; Lu, G.; Zhang, X.; Song, S.; Zhang, X.; et al. Migration-Enhanced Epitaxial Growth of InAs/GaAs Short-Period Superlattices for THz Generation. *Nanomaterials* **2024**, *14*, 294. [[CrossRef](#)] [[PubMed](#)]
- Berry, C.W.; Hashemi, M.R.; Jarrahi, M. Generation of High Power Pulsed Terahertz Radiation Using a Plasmonic Photoconductive Emitter Array with Logarithmic Spiral Antennas. *Appl. Phys. Lett.* **2014**, *104*, 081122. [[CrossRef](#)]
- Kostakis, I.; Saeedkia, D.; Missous, M. Terahertz Generation and Detection Using Low Temperature Grown InGaAs-InAlAs Photoconductive Antennas at 1.55 μ m Pulse Excitation. *IEEE Trans. THz Sci. Technol.* **2012**, *2*, 617–622. [[CrossRef](#)]
- Wang, Y.; Kostakis, I.; Saeedkia, D.; Missous, M. Optimised THz Photoconductive Devices Based on Low-temperature Grown III-V Compound Semiconductors Incorporating Distributed Bragg Reflectors. *IET Optoelectron.* **2017**, *11*, 53–57. [[CrossRef](#)]
- Warren, A.C.; Woodall, J.M.; Freeouf, J.L.; Grischkowsky, D.; McInturff, D.T.; Melloch, M.R.; Otsuka, N. Arsenic Precipitates and the Semi-Insulating Properties of GaAs Buffer Layers Grown by Low-Temperature Molecular Beam Epitaxy. *Appl. Phys. Lett.* **1990**, *57*, 1331–1333. [[CrossRef](#)]
- Ibbetson, J.P.; Ibbetson, J.; Speck, J.S.; Gossard, A.C.; Mishra, U.K. Observation of Arsenic Precipitates in GaInAs Grown at Low Temperature on InP. *Appl. Phys. Lett.* **1993**, *62*, 2209–2211. [[CrossRef](#)]
- Lilienthal-Weber, Z.; Swider, W.; Yu, K.M.; Kortright, J.B.; Smith, F.W.; Calawa, A.R. Breakdown of Crystallinity in Low-Temperature-Grown GaAs Layers. *Appl. Phys. Lett.* **1991**, *58*, 2153–2155. [[CrossRef](#)]
- Yao, T. A New High-Electron Mobility Monolayer Superlattice. *Jpn. J. Appl. Phys.* **1983**, *22*, L680. [[CrossRef](#)]
- Globisch, B.; Dietz, R.J.B.; Stanze, D.; Göbel, T.; Schell, M. Carrier Dynamics in Beryllium Doped Low-Temperature-Grown InGaAs/InAlAs. *Appl. Phys. Lett.* **2014**, *104*, 172103. [[CrossRef](#)]
- Kostakis, I.; Saeedkia, D.; Missous, M. Characterization of Low Temperature InGaAs-InAlAs Semiconductor Photo Mixers at 1.55 μ m Wavelength Illumination for Terahertz Generation and Detection. *J. Appl. Phys.* **2012**, *111*, 103105. [[CrossRef](#)]
- Missous, M. Advanced MBE Low Temperature Grown Materials for CW THz Generation and Detection. In Proceedings of the 2011 IEEE SENSORS Proceedings, Limerick, Ireland, 28–31 October 2011; IEEE: Limerick, Ireland, 2011; pp. 184–186.
- Gerard, J.M.; Marzin, J.Y.; d’Anterrosches, C.; Soucaïl, B.; Voisin, P. Optical Investigation of the Band Structure of InAs/GaAs Short-Period Superlattices. *Appl. Phys. Lett.* **1989**, *55*, 559–561. [[CrossRef](#)]
- André, J.P.; Deswarte, A.; Lugagne-Delpon, E.; Voisin, P.; Ruterana, P. High Electron Mobility in (InAs) n (GaAs) n Short Period Superlattices Grown by MOVPE for High-Electron Mobility Transistor Structure. *J. Electron. Mater.* **1994**, *23*, 141–146. [[CrossRef](#)]

25. Tadayon, B.; Tadayon, S.; Spencer, M.G.; Harris, G.L.; Griffin, J.; Eastman, L.F. Increase of Electrical Activation and Mobility of Si-Doped GaAs, Grown at Low Substrate Temperatures, by the Migration-Enhanced Epitaxy Method. *J. Appl. Phys.* **1990**, *67*, 589–591. [[CrossRef](#)]
26. Gérard, J.M.; Marzin, J.Y.; Jusserand, B. Modulated Molecular Beam Epitaxy: A Successful Route toward High Quality Highly Strained Heterostructures. *J. Cryst. Growth* **1991**, *111*, 205–209. [[CrossRef](#)]
27. Gérard, J.M.; Marzin, J.Y.; Jusserand, B.; Glas, F.; Primot, J. Structural and Optical Properties of High Quality InAs/GaAs Short-Period Superlattices Grown by Migration-Enhanced Epitaxy. *Appl. Phys. Lett.* **1989**, *54*, 30–32. [[CrossRef](#)]
28. Camacho-Reynoso, M.; Hernández-Gutiérrez, C.A.; Yee-Rendón, C.M.; Rivera-Rodríguez, C.; Bahena-Urbe, D.; Gallardo-Hernández, S.; Kudriavtsev, Y.; López-López, M.; Casallas-Moreno, Y.L. Cubic In_xGa_{1-x}N/GaN Quantum Wells Grown by Migration Enhanced Epitaxy (MEE) and Conventional Molecular Beam Epitaxy (MBE). *J. Alloys Compd.* **2022**, *921*, 165994. [[CrossRef](#)]
29. Gerard, J.-M.; Marzin, J.Y. High Quality Ultrathin InAs/GaAs Quantum Wells Grown by Standard and Low-temperature Modulated-fluxes Molecular Beam Epitaxy. *Appl. Phys. Lett.* **1988**, *53*, 568–570. [[CrossRef](#)]
30. Gerard, J.M.; Marzin, J.Y.; d'Anterrosches, C.; Soucaill, B.; Voisin, P. Optical Study of the Band Structure of InAs/GaAs Ordered Alloys. *Surf. Sci.* **1990**, *229*, 456–458. [[CrossRef](#)]
31. Colvard, C.; Gant, T.A.; Klein, M.V.; Merlin, R.; Fischer, R.; Morkoc, H.; Gossard, A.C. Folded Acoustic and Quantized Optic Phonons in (GaAl)As Superlattices. *Phys. Rev. B* **1985**, *31*, 2080–2091. [[CrossRef](#)]
32. Emura, S.; Soni, R.K.; Gonda, S. Interfacial Stress in Strained-Ultrathin-Layer (InAs)₂/(GaAs)₁ Superlattice. *Phys. Rev. B* **1992**, *46*, 1463–1467. [[CrossRef](#)]
33. Bradshaw, J.; Song, X.J.; Shealy, J.R.; Zhu, J.G.; O/stergaard, H. Characterization by Raman Scattering, x-Ray Diffraction, and Transmission Electron Microscopy of (AlAs)_m (InAs)_m Short Period Superlattices Grown by Migration Enhanced Epitaxy. *J. Appl. Phys.* **1992**, *72*, 308–310. [[CrossRef](#)]
34. Scamarcio, G.; Brandt, O.; Tapfer, L.; Mowbray, D.J.; Cardona, M.; Ploog, K. Structural and Vibrational Properties of (InAs)_m (GaAs)_n Strained Superlattices Grown by Molecular Beam Epitaxy. *J. Appl. Phys.* **1991**, *69*, 786–792. [[CrossRef](#)]
35. Arbia, B.M.; Demir, I.; Kaur, N.; Saidi, F.; Zappa, D.; Comini, E.; Altuntaş, I.; Maaref, H. Experimental Insights toward Carrier Localization in In-Rich InGaAs/InP as Candidate for SWIR Detection: Microstructural Analysis Combined with Optical Investigation. *Mater. Sci. Semicond. Process.* **2023**, *153*, 107149. [[CrossRef](#)]
36. Smiri, B.; Saidi, F.; Mlayah, A.; Mâaref, H. Comparative Optical Studies of InAlAs/InP Quantum Wells Grown by MOCVD on (311)A and (311)B InP Planes. *J. Mater. Sci. Mater. Electron.* **2020**, *31*, 10750–10759. [[CrossRef](#)]
37. Min, K.-I.; Rho, H.; Song, J.D.; Choi, W.J.; Lee, Y.T. Raman Studies of InGaAlAs Digital Alloys. *J. Korean Phys. Soc.* **2011**, *59*, 2801–2805. [[CrossRef](#)]
38. Chen, X.; Gu, Y.; Zhang, Y.G.; Ma, Y.; Xi, S.; Du, B.; Di, Z.; Ji, W.; Shi, Y. Optical Characterization of Si-doped Metamorphic InGaAs with High Indium Content. *Phys. Status Solidi B-Basic Solid State Phys.* **2017**, *254*, 1700094. [[CrossRef](#)]
39. Kim, N.; Han, S.-P.; Ko, H.; Leem, Y.A.; Ryu, H.-C.; Lee, C.W.; Lee, D.; Jeon, M.Y.; Noh, S.K.; Park, K.H. Tunable Continuous-Wave Terahertz Generation/Detection with Compact 1.55 μm Detuned Dual-Mode Laser Diode and InGaAs Based Photomixer. *Opt. Express* **2011**, *19*, 15397–15403. [[CrossRef](#)]
40. Harmon, E.S.; Melloch, M.R.; Woodall, J.M.; Nolte, D.D.; Otsuka, N.; Chang, C.L. Carrier Lifetime versus Anneal in Low Temperature Growth GaAs. *Appl. Phys. Lett.* **1993**, *63*, 2248–2250. [[CrossRef](#)]
41. Sfuncia, G.; Nicotra, G.; Giannazzo, F.; Péc, B.; Gueorguiev, G.K.; Kakanakova-Georgieva, A. 2D Graphitic-like Gallium Nitride and Other Structural Selectivity in Confinement at the Graphene/SiC Interface. *CrystEngComm* **2023**, *25*, 5810–5817. [[CrossRef](#)]

Disclaimer/Publisher's Note: The statements, opinions and data contained in all publications are solely those of the individual author(s) and contributor(s) and not of MDPI and/or the editor(s). MDPI and/or the editor(s) disclaim responsibility for any injury to people or property resulting from any ideas, methods, instructions or products referred to in the content.